THE ASTROPHYSICAL JOURNAL, 517:460–471, 1999 May 20

SIMULTANEOUS DUAL-FREQUENCY OBSERVATIONS OF GIANT PULSES FROM THE CRAB PULSAR

SHAUNA SALLMEN AND D. C. BACKER
University of California, Berkeley, CA 94720-3411; ssallmen@astro.berkeley.edu, dbacker@astro.berkeley.edu
T. H. HANKINS
New Mexico Institute of Mining & Technology, Socorro, NM 87801; thankins@aoc.nrao.edu
D. MOFFETT
Physics Department, University of Tasmania, GPO Box 252-21, Hobart, Tasmania 7001, Australia; David.Moffett@utas.edu.au
AND
S. LUNDGREN
MS4051, Lockheed Martin Astronautics, P.O. Box 179, Denver, CO 80201-0179; Scott.C.Lundgren@lmco.com
Received 1998 August 19; accepted 1998 December 29

ABSTRACT

Simultaneous measurements of giant pulses from the Crab pulsar were taken at two widely spaced frequencies, using the real-time detection of a giant pulse at 1.4 GHz at the Very Large Array to trigger the observation of that same pulse at 0.6 GHz at a 25 m telescope in Green Bank, WV. Interstellar dispersion of the signals provided the necessary time to communicate the trigger across the country via the Internet. About 70% of the pulses are seen at both 1.4 and 0.6 GHz, implying an emission mechanism bandwidth of *at least* 0.8 GHz at 1 GHz for pulse structure on timescales of 1 to 10 μs. The giant pulse spectral indices fall between -2.2 and -4.9, which may be compared to the average main pulse value for this pulsar of -3.0. The arrival times at both frequencies display a jitter of 100 μs within the window defined by the average main pulse profile and are tightly correlated. This tight correlation places limits on both the emission mechanism and the frequency-dependent propagation within the magnetosphere. At 1.4 GHz, the giant pulses are resolved into several closely spaced components. Simultaneous observations at 1.4 and 4.9 GHz show that the component splitting is frequency independent. We conclude that the multiplicity of components is intrinsic to the emission from the pulsar, and reject the hypothesis that this is the result of multiple imaging as the signal propagates through the perturbed thermal plasma in the surrounding nebula. At both 1.4 and 0.6 GHz, the pulses are characterized by a fast rise time and an exponential decay time that are correlated. At 0.6 GHz, the rise time is not resolved. The rise and fall times of the 1.4 GHz components vary from component to component and from pulse to pulse. The pulse broadening, with its exponential decay form, is most likely the result of multipath propagation in intervening ionized gas. These decay times, and that seen in contemporaneous 0.3 GHz average pulse data, are large compared to normal conditions for the Crab pulsar. The most likely location for the perturbed plasma is the interface region between the pulsar-driven synchrotron nebula and the overlying supernova ejecta.

Subject headings: pulsars: individual (Crab Pulsar) — radiation mechanisms: nonthermal — scattering — supernova remnants

1. INTRODUCTION

The Crab pulsar was discovered in 1968 by the detection of its extremely strong individual pulses (Staelin & Reifenstein 1968). Such pulses, which are hundreds of times stronger than the average, are not seen in most pulsars. The properties of these giant pulses have been explored for many years (e.g., Heiles, Campbell, & Rankin 1970; Staelin & Sutton 1970; Friedman & Boriakoff 1990; Lundgren et al. 1995). Giant pulses in the Crab pulsar occur at all radio frequencies, but only at the rotational phase of the main pulse and interpulse components. These two components have counterpart nonthermal emission at high frequencies (from the infrared to gamma-ray energies), and may be associated with the outer voltage gaps in the pulsar magnetosphere (Romani & Yadigaroglu 1995). Giant pulses are not seen in the radio precursor nor at the phases of the high radio frequency components recently described by Moffett & Hankins (1996). The radio precursor is identified as being more typical of the emission from a conventional pulsar, and is believed to originate at, and be aligned with, the magnetic pole.

Lundgren et al. (1995) found that two separate distributions were required to describe the fluctuations of single pulse energies[1] for the Crab pulsar main pulse and interpulse components at 0.8 GHz. About 2.5% of the pulses lie in the giant pulse distribution, with a power-law slope extending to high values and a low-energy cutoff of 20 times the average of all pulse energies. The distinct distributions suggest different emission mechanisms for the giant and weak pulses, and possibly different emission locations within the magnetosphere. However, the lack of an offset in the timing residuals between giant pulses and the average pulse profile (Lundgren 1994; for opposing evidence see Friedman & Boriakoff 1990) suggests that the emission region is the same.

[1] Pulsar emission profiles are generally given in units of *flux* (Jy), even though in the context of rotating neutron stars one actually samples a one-dimensional cut of the *specific intensity* pattern (Jy sr^{-1}). The integral of emission over a pulse component in the latter case would be its flux, while in the former and conventional case one quantifies the integrated component emission in units of energy (Jy-s).

The frequency of occurrence (f_o) of pulses with energy greater than 20 times the average increases with frequency, from 10^{-4} at 0.146 GHz (Argyle & Gower 1972) to 0.025 at 0.8 GHz (Lundgren et al. 1995). The contribution of the giant pulses to the average energy of all pulses also increases with radio frequency, although not as quickly. The probability distribution of the giant pulse energies can be written as

$$P(E_{\rm GP} > E_o) = f_o \left(\frac{E_o}{E_{\rm min}} \right)^{-\alpha},$$

where f_o is the frequency of occurrence of the giant pulses, and $E_{\rm min}$ is the minimum energy. Correspondingly, the probability density function is

$$p(E_{\rm GP}) = \frac{f_o \alpha}{E_{\rm min}} \left(\frac{E_{\rm GP}}{E_{\rm min}} \right)^{-\alpha-1},$$

and the corresponding mean giant-pulse energy averaged over all pulses is $[(f_o \alpha)/(\alpha - 1)]E_{\rm min}$. The probability distribution P has a slope $\alpha = 2.3 \pm 0.15$ at 0.8 GHz (Lundgren et al. 1995), and $\alpha = 2.5$, with significant errors, at 0.146 GHz (Argyle & Gower 1972). At 1.4 and 0.43 GHz the overall slope is roughly consistent with these, but is not the same for all energies (Friedman & Boriakoff 1990; Moffett 1997). Using the scaling law $\alpha \approx 2.5$ at all radio frequencies below 0.8 GHz, we find that the contribution of giant pulses with energy more than 20 times the average of all pulses, $E_{\rm GP} > 20E_{\rm avg}$, is 89% of the average energy at 0.8 GHz (Lundgren et al. 1995), 9% at 0.43 GHz (Friedman & Boriakoff 1990), and only about 1% at 0.146 GHz (Argyle & Gower 1972). At 1.4 GHz, a similarly large fraction of the energy comes from the approximately 2% of pulses with greater than 20 times the average energy, although a single slope α does not accurately describe the distribution.

There is no evidence of increased flux density in pulses near the giant pulses (Sutton, Staelin, & Price 1971; Lundgren 1994), nor is there any correlation between giant pulses. We note that many pulsars do show pulse-to-pulse correlation, indicating a memory process with a duration of many rotational periods. The timescale of giant pulses is, in contrast, less than a single period. In addition, the time separation distribution for giant pulses is consistent with a Poisson process (Lundgren 1994).

Despite all these studies, the emission bandwidth of the giant pulses has been poorly determined. Comella et al. (1969) found that 50% of giant pulses were seen simultaneously at 0.074 and 0.111 GHz. Goldstein & Meisel (1969) also found that some but not all pulses were correlated between 0.112 and 0.170 GHz. Sutton et al. (1971) noted that there was no evidence that the largest pulses at 0.16 and 0.43 GHz were correlated. Heiles & Rankin (1971) observed giant pulses simultaneously at 0.318 and 0.111 GHz, for a bandwidth spread of about 3:1. They found that pulses classified as giant at one frequency were stronger than the average at the other, but not usually classified as giant. Much more recently, Moffett (1997) reported that fully 90% of the giant pulses detected at 4.9 GHz were also detected at 1.4 GHz, implying an emission bandwidth of 3.5 GHz at high radio frequencies. In this paper, we report on giant pulses observed simultaneously at 1.4 and 0.6 GHz to explore the correlation in this intermediate range of frequencies. Section 2 describes the observations, while an analysis of the simultaneous pulses is given in § 3.

2. OBSERVATIONS

The data shown here were recorded on 1996 May 21 at UT $17^{\rm h}45^{\rm m}$–$19^{\rm h}15^{\rm m}$ (1.4/0.6 GHz) and 1996 October 12 at UT $11^{\rm h}30^{\rm m}$–$12^{\rm h}05^{\rm m}$ (4.9/1.4 GHz). We also refer to observations at 1.4 GHz earlier in 1996 and in 1997 November. The 1.4 and 4.9 GHz data were taken at the NRAO Very Large Array (VLA).[2] For the simultaneous 1.4/0.6 GHz observations, all 27 VLA antennas were phased to create the equivalent sensitivity of a 130 m antenna, while the 0.6 GHz data were taken using a 25 m telescope at the NRAO Green Bank, WV, site. For the simultaneous 4.9/1.4 GHz observations, the VLA was split into two equal subarrays.

The peculiar phases of each antenna at the VLA were determined by observing a standard point-source calibrator. These phases were then applied to the antennas to synthesize a pencil beam pointed at the Crab pulsar, which essentially resolves out the bright Crab Nebula and vastly improves the signal-to-noise ratio compared to a single-dish antenna. The received voltages from each antenna are summed to form orthogonally circularly polarized 50 MHz bandwidth signals centered at precisely 4.8851 or 1.4351 GHz. The signals are then detected and summed with a 100 μs time constant. The detector rms noise power was determined using an rms to DC converter. A detector threshold was set at either 5 or 6 times the running average of this rms noise level. Pulses that exceeded this threshold generated a trigger that was sent to the data recorder; these pulses were then saved to disk and archived to tape using the full 50 MHz bandwidth. In an off-line computer, the data were coherently dedispersed using the method developed by Hankins (1971) and described by Hankins & Rickett (1975). Although the ultimate time resolution of the dedispersed data is 10 ns, for the analyses described here the data were smoothed to 0.5–1.0 μs after software detection.

The two linearly polarized signals centered at exactly 0.610 GHz were converted to 90 and 110 MHz center frequencies, respectively. The two intermediate-frequency signals were then summed and transmitted on a single fiber-optic link from the 25 m telescope to the Green Bank–Berkeley Pulsar Processor (GBPP),[3] which was located at the 140 ft telescope. The GBPP converted the signals to baseband, split these into 32 0.5 MHz channels, and dedispersed the pulsar signal in each channel by (de)convolution in the time domain. The dispersion delay across the 16 MHz bandwidth of the GBPP at 0.6 GHz is about 33 ms, or one pulse period for the dispersion measure of the Crab pulsar (DM ≈ 56.8 pc cm^{-3}). Full Stokes information for 982 samples across the pulsar period was recorded with an accurate UTC start time for each pulse. The 25 m telescope also monitors the Crab pulsar daily with 0.327 GHz observations, which are valuable for their sensitivity to scatter broadening by intervening plasma.

The 1.4/0.6 GHz part of this experiment utilized the difference in pulse arrival time between the two frequencies due to interstellar dispersion to provide the time interval needed to communicate the trigger information between the sites. At the VLA, the same trigger pulse that was sent to the

[2] The National Radio Astronomy Observatory is a facility of the National Science Foundation operated under cooperative agreement by Associated Universities, Inc.

[3] A partial technical description of the GBPP is given in (Backer et al. 1997).

data recorder was also sent, as an interrupt, to the SUN workstation used for experiment control and recording. The program that received the interrupt had a socket link open over the Internet to a slave program running on another SUN workstation in Green Bank, and communicated the 1.4356 GHz arrival time of the pulse to Green Bank.

We arranged for the GBPP to begin taking data just before the giant pulse reached the upper edge of the 0.6 GHz band, in order to obtain data for the same main pulse across the entire band. The dispersion time delay between 1.4351 and 0.618 GHz (the top of our 0.6 GHz band) allowed a half second (0.503 s) to arrange this. The SUN workstations at the two sites were synchronized to the local versions of UTC, which were derived from accurate atomic clocks using the xntp protocol. Although both remote sites had 56 kB links to the Internet, the typical Internet transfer time delay was 200 ms during our observation. The program running in Green Bank received the trigger message with its VLA time stamp, calculated the transit time of the trigger, and compared that to the dispersion delay difference of 0.503 s. In addition to this delay, the program included other factors such as the difference in pulse arrival due to the separation between observing sites on the Earth and the latency in the GBPP hardware, both of which were on the order of 1–3 ms. If sufficient time remained, the program waited until the appropriate time and issued a trigger to the GBPP via the SUN parallel port to take data for the next pulse period. Owing to the slow rate of data transfer from the GBPP, it could only accept such a command approximately every 12 s. Some VLA-initiated triggers were therefore missed by the GBPP.

For the 4.9/1.4 GHz measurements, the recording system was triggered by a 4.9 GHz pulse, and then automatically triggered again after the appropriate dispersion delay to record the 1.4 GHz signals.

The Stokes parameters for the high time resolution data from the VLA were formed from the dedispersed voltages. The necessary 90° phase shift was obtained using a finite impulse response approximation to the Hilbert transform and was applied to the right-circular polarization signal before forming the Stokes parameters. No instrumental polarization corrections were made other than bandpass leveling and gain matching. Concurrent calibration (Moffett 1997) has shown that the polarization cross-coupling is less than 10% for the VLA phase array. The polarization error is then comparable with the radiometer uncertainty imposed by the limited number of degrees of freedom in the data $[\sigma_I/I = (4\Delta\nu\,\Delta\tau)^{-1/2} = 0.1]$.

The polarization profiles at 0.6 GHz were calibrated using factors derived from pulsed-noise observations. The receiver introduces a relative phase between the two linear polarizations which couples the Stokes parameters U and V. This phase was determined and removed using nearby observations of the Vela pulsar and comparison to a template polarization profile. No attempt has been made to remove coupling between the two polarizations. The error in polarization due to improper calibration is estimated at 10%. For each pulse, the relative dispersion between the 32 channels was removed, and the resulting data were summed over channels, after first removing the effects of the pulsar's rotation measure ($\mathrm{RM} = -42.3$ rad m^{-2}) across the band. The unknown Faraday rotation from the ionosphere causes negligible rotation of 1° to 10° across the total band.

3. ANALYSIS

3.1. *Wide Bandwidth Correlation*

Of the 85 trigger events initiated at the VLA, a total of 77 events reached Green Bank within the required time and were accepted by the GBPP. The xntp protocol requires 24 hours to stabilize to the accuracy required by our experiment. The minimum time stabilization period was not available for the SUN at the VLA. Consequently, the VLA clock used to identify the time at which the trigger was sent drifted by a small amount. We are currently certain that the received trigger events allowed capture of the correct period in the GBPP for 42 pulses.

The arrival times and pulse energy amplitudes were determined at both frequencies for each of these pulses. The 0.6 GHz arrival times were determined by cross correlation with a model template, which consisted of a single-sided exponential with a decay timescale of three time bins, about 100 μs. Owing to the complex structure discussed below, the 1.4 GHz pulse arrival times were obtained by computing the location of the centroid of the pulses. Pulse amplitudes in units of Jy-s were determined by removing an "off-pulse" baseline, and then summing the flux in the time bins that comprise the "on-pulse" window. The measurement uncertainty of these amplitudes was determined from the off-pulse noise distribution.

We definitely detected 29 of the 42 correctly timed pulses at both radio frequencies. These detections correspond to a 0.6 GHz pulse energy threshold of about 4.5 times the typical measurement uncertainty, or 0.075 Jy-s using 0.14 K Jy^{-1} for the 25 m telescope. This gain factor was determined using on and off measurements of the Crab nebula (which is 1208 Jy at 0.6 GHz), and has an estimated uncertainty of 50%. We conclude that about 70% of the pulses are detected at both frequencies. This statistic is used to discuss the spectral index distribution below.

The data for a single giant pulse at 1.4 and 0.6 GHz are displayed in Figures 1 and 2, respectively. This pulse is strongly polarized at both frequencies, although fully two-thirds of the giant pulses at the lower frequency are consistent with zero polarization. The 0.6 GHz data has a low number of degrees of freedom, and so the polarization estimation uncertainty is about 5%. At 1.4 GHz, the typical polarization is about 8%, although at least one pulse is 50% polarized. The position angle of the linear polarization generally varies significantly across the pulse, as seen in Figure 1.

The arrival times for the 29 giant pulses detected at the two frequencies were separately compared to a single model for this pulsar using the TEMPO program developed for pulsar timing (Taylor & Weisberg 1989). For each radio frequency, the arrival times are well represented by the model, leaving timing residuals of the order of ± 100 μs. The residuals are comparable to the pulse width of the average profile during periods of low scattering, which is 275 ± 50 μs (FWHM) at 0.6 GHz and 257 ± 50 μs at 1.4 GHz. These widths were estimated using GBPP data obtained with the 25 m and 140 ft telescopes, respectively.

The timing residuals for 1.4 and 0.6 GHz are plotted against one another in the top panel of Figure 3, which shows that they are highly correlated. The solid line has a slope of 1 and goes through the origin. In order for the

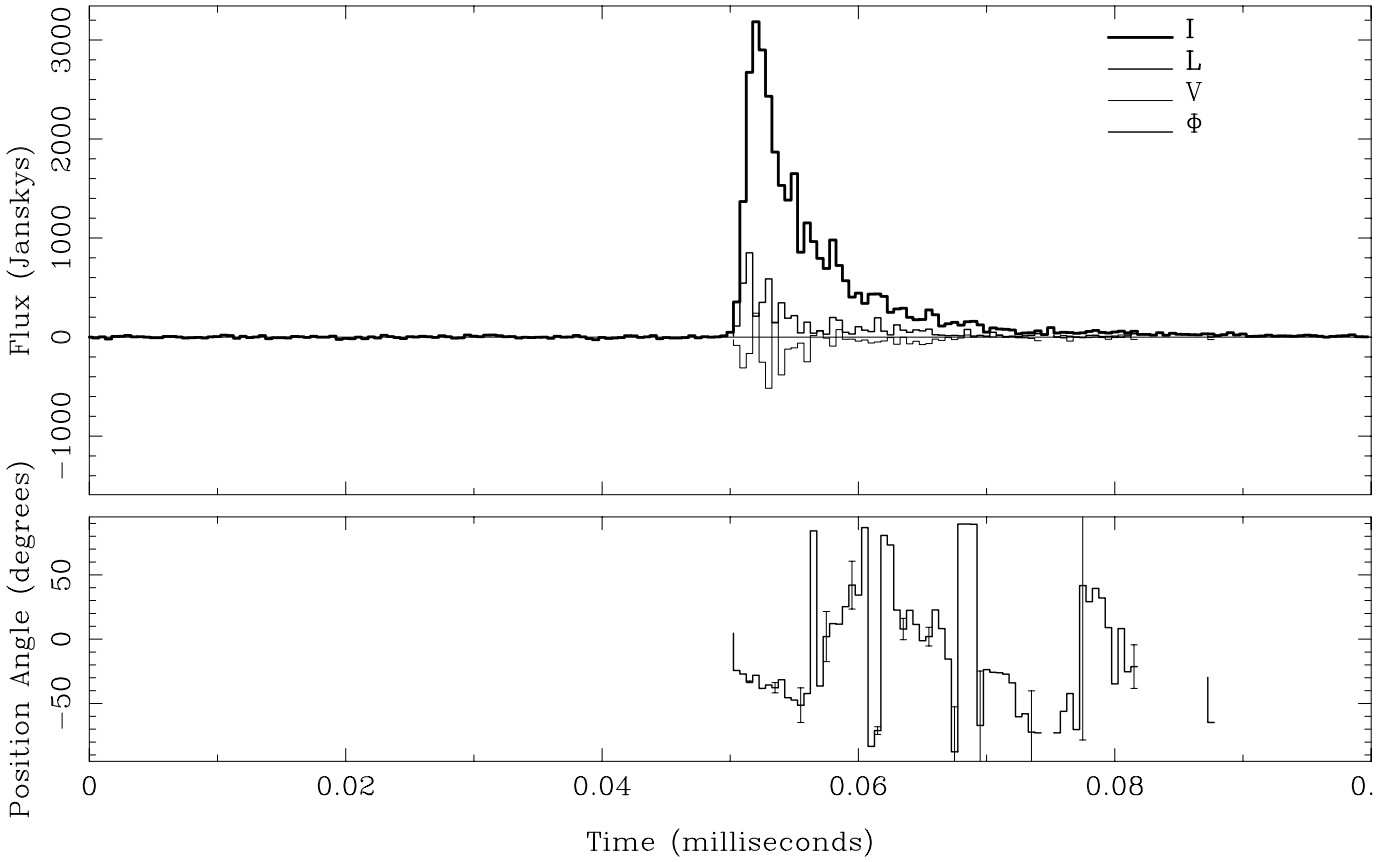

FIG. 1.—*Top*: total intensity I, along with linear and circular polarizations L and V, for a single giant pulse at 1.4 GHz, taken at the VLA on 1996 May 21, with a temporal resolution of 0.5 μs. The vertical scale indicates that this pulse reached a peak flux of 3000 Jy. *Bottom*: linear polarization position angle wherever $L > 3$ times the off-pulse rms noise.

points to fall along this line, the 1.049 ms digital latency of the GBPP and the 235.42 μs latency of the VLA samplers and delay lines were removed, and a further fit for dispersion measure was done in TEMPO. The derived DM is 56.830 pc cm^{-3}, although systematic errors may remain in the arrival times from the two sites. The bottom panel of Figure 3 displays the same 1.4 GHz residuals with the solid line removed.

Eilek (1996) has shown that the dispersion law in the polar cap is proportional to ν^{-1}, as opposed to ν^{-2} for the cold interstellar medium (ISM). No systematic trends remain in the data in the lower panel of Figure 3, indicating that systematic variations with pulse phase are less than ± 15 μs between our two bands. This places limits on the differential effects of propagation through the magnetosphere. Geometrically, emission in the two bands must originate within $0^{\circ}.16$ of rotational phase, or a range of 4.5 km in altitude. It would have been possible to have correlated emission from subpulses at different pulse longitudes at each frequency. In this case, the radiation at the two frequencies need not have come from the same radiating unit of charges. The observed rms jitter in arrival time at either frequency is ≈ 100 μs, so the fact that the difference between the residuals has such a small dispersion indicates that the emission must be from the same radiating unit at both frequencies. This means that at least 70% of the giant pulses must have a bandwidth of *at least* 0.8 GHz at 1 GHz. The emission is clearly broadband for these cases.[4]

3.2. *Pulse Shape Model*

The giant pulses at 0.6 GHz all have profiles that display a fast rise followed by an exponential decay, similar to the profile shown in Figure 2. The exponential decay timescale is $\tau_{\rm ISS}(0.6\ {\rm GHz}) = 95 \pm 5$ μs. Monitoring of the exponential broadening of the average pulse profile at 0.3 GHz using the 25 m telescope (Backer & Wong 1996) provides a contemporaneous decay timescale of $\tau_{\rm ISS}(0.3\ {\rm GHz}) = 1.3 \pm 0.2$ ms. The 0.3 and 0.6 GHz pulse-broadening timescales are consistent with the $\nu^{-4\ {\rm to}\ -4.4}$ dependence expected from scattering by an intervening turbulent plasma screen. At the time of these observations, the Crab was undergoing a period of unusually large scattering. The contemporaneous value of $\tau_{\rm ISS}(0.3\ {\rm GHz})$ may be compared to 0.28 ms at an earlier epoch. Enhanced scattering of the Crab pulsar radiation also occurred in 1975 (Isaacman & Rankin 1977;

[4] Note that in this paper the term "broadband" connotes simultaneous emission over wide range of radio frequencies with a ratio of amplitudes comparable to that of the average pulse. However, the observed emission has a very steep spectrum, even if weighted by frequency to obtain total power, and is therefore narrowband in an absolute sense.

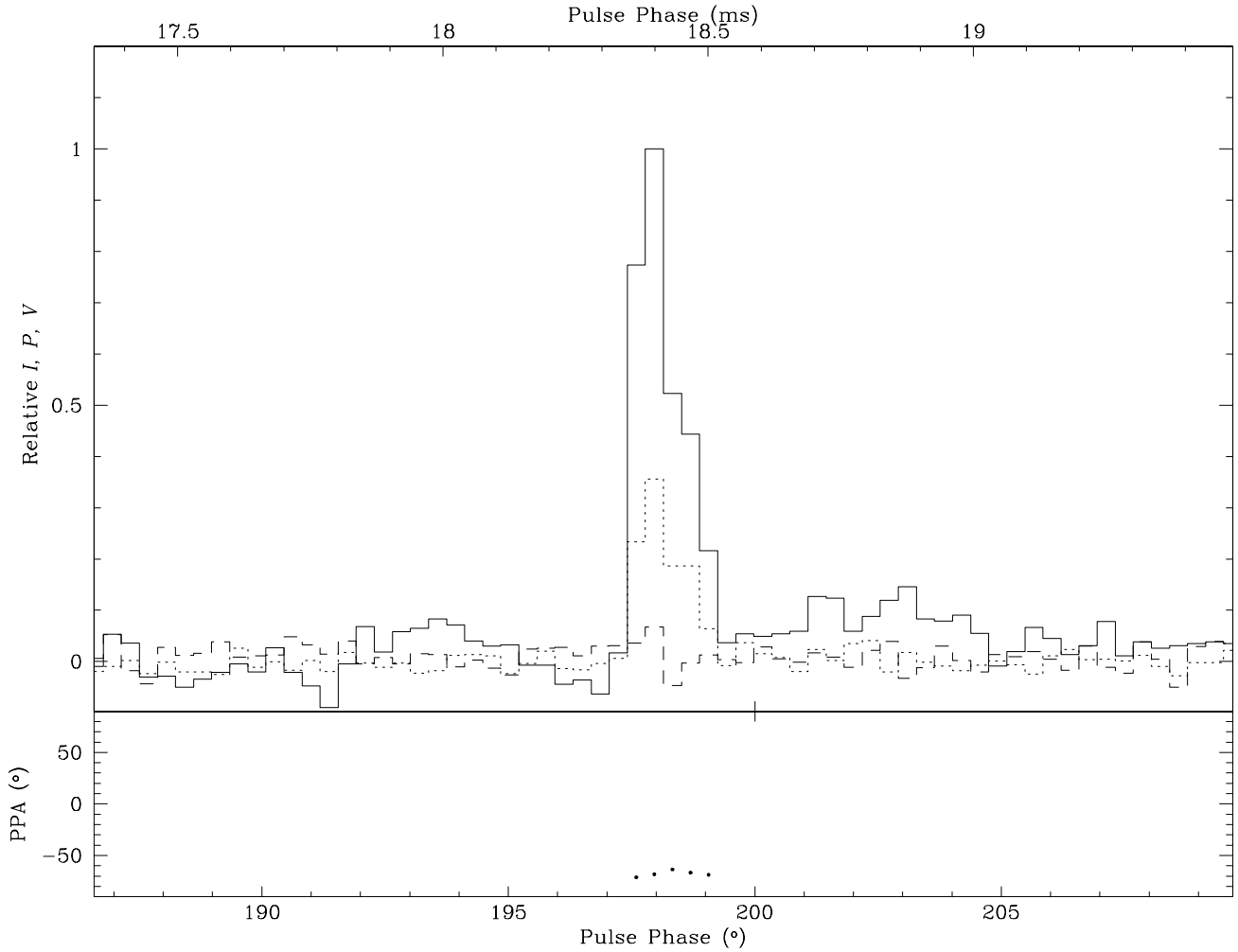

FIG. 2.—*Top*: relative values at 0.6 GHz of the total intensity I, and the linear and circular polarizations L and V, for the same single pulse as shown in Fig. 1, taken with the GBPP. The temporal resolution is approximately 34 μs. The peak flux for this pulse was $\approx$7000 Jy. The negative and positive features on either side of the main peak are artifacts due to the nonlinear response of the GBPP. *Bottom*: linear polarization position angle wherever $L > 3$ times the off-pulse rms noise.

Lyne & Thorne 1975). A likely site of the perturbed plasma that causes the enhanced pulse broadening is in the interface between the synchrotron nebula and the supernova ejecta (Hester et al. 1996). This region is proposed because such enhanced scattering events are not seen for any other pulsar. Furthermore, this location is known to contain dense thermal plasma with structure on a variety of length scales. The transverse velocity of the line of sight with respect to the interface material is sufficient to bring occasional regions that produce strong perturbations into view. The fast rise of the 0.6 GHz giant pulses indicates that any intrinsic timescale of the pulse is unresolved, $\lesssim 10$ μs.

The giant pulses at 1.4 GHz have a wide variety of shapes. Figures 4 and 5 display two further single-pulse profiles. The first pulse is extremely narrow and is dominated by a single component, while the second has several components contributing to the emission. The darker solid line shows a fit to the data, where the flux model $S(t)$ consists of up to six components and is of the form

$$S(t) = \sum_{i=1}^{n} a_{1_i}(t - a_{2_i})e^{-(t-a_{2i})/a_{3i}}, \quad n \leq 6 . \qquad (1)$$

These components rise to their peak in a time a_3, fall by e^{-1} in a further $2.15a_3$, and have a pulse energy amplitude of $A = a_1 a_3^2$. At 1.4 GHz, the majority of giant pulse components are well represented by this model, with widths a_3 ranging from 1.2 to 10 μs. Components with widely varying decay timescales may be superposed within a single giant pulse, as shown in Figure 5. The narrow component of the giant pulse shown in Figure 4 has a rise time of 1.2 μs, and a decay timescale of 2.5 μs. The weak and broad second component in Figure 4 is clearly necessary to account for the emission on the trailing edge of the pulse, which does not follow an exponential tail.

3.3. *Pulse Shape Interpretation*

The 1.4 GHz observations raise fundamental issues about the nature of the giant pulse emission. Is the multiplicity of the components and the characteristic shape of the components a result of propagation through a turbulent screen, or are these effects intrinsic to pulse formation and propagation in the pulsar magnetosphere, or is there a mixture of effects present? Two additional results from further observations at the VLA and the 0.3 GHz monitoring in Green Bank provide important constraints to aid in answering these questions.

The first observational constraint arises from our broadening measurement of 1.3 ms at 0.3 GHz, which scales

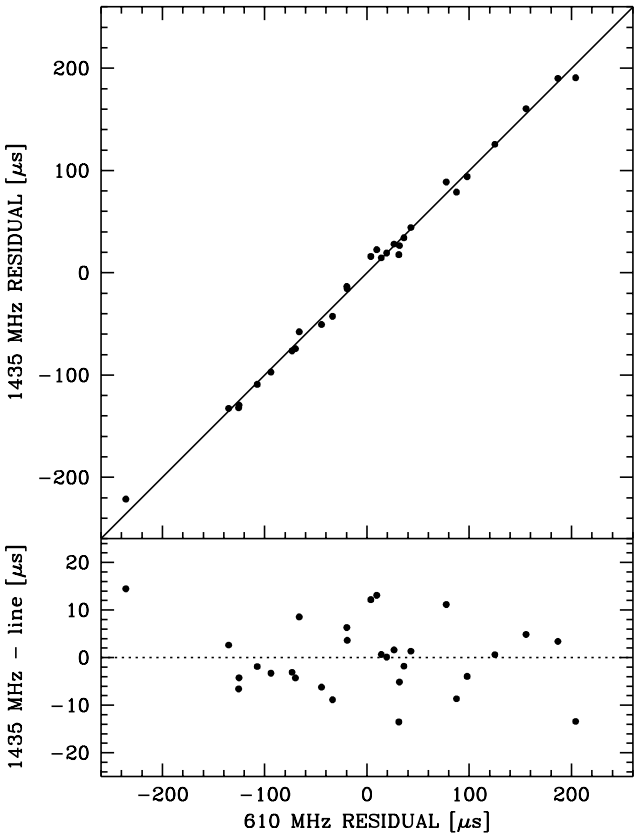

FIG. 3.—*Top*: 1.4 GHz timing residuals vs. 0.6 GHz timing residuals. The solid line passes through the origin with slope 1. *Bottom*: The same data with this line removed.

to 1.9–3.5 μs at 1.4 GHz using the $\nu^{-4\text{ to }-4.4}$ dependence expected for a spectrum of turbulence filling the intervening screen. This range is consistent with the typical *minimum* broadening time of approximately 2.5 μs that we measured for the giant pulses at 1.4 GHz. During a later epoch (1997 November 26), when the scattering broadening of the average pulse at 0.3 GHz had increased dramatically by a factor of about 5, the minimum pulse widths of the 1.4 GHz giant pulses increased by a similar factor. At an earlier epoch in 1996, both the 0.3 GHz average pulse broadening and the minimum width of the 1.4 GHz giant pulses were reduced.

The second observational constraint on our interpretation of the 1.4 GHz giant pulse shapes comes from a consideration of the multiple component spacings. These do not scale in the same way as the component broadening. During an earlier epoch of low 0.3 GHz scattering, the typical 1.4 GHz component spacing is similar to that for 1996 May 21. In addition, simultaneous VLA measurements of the giant pulses at 1.4 and 4.9 GHz (1996 October 12) show a frequency *independence* of the multiple component spacing (Hankins & Moffett 1998). At 4.9 GHz, the pulse components are intrinsically very short, typically 0.1 to 0.4 μs wide, while the corresponding components are broadened at 1.4 GHz. Simultaneous 4.9 and 1.4 GHz measurements of a single giant pulse are shown in Figures 6*a* and 6*b*. The separation of the two main components is similar at both frequencies, in that the onsets of the pulse components (the fiducial points in the fits discussed in § 3.2) are separated by the same amount. A similar conclusion about the frequency independence of structure can be inferred from the 1.4 and 0.6 GHz measurements of 1996 May 21; that is, 1.4 GHz giant pulses with multiple components have a spread of tens of microseconds, which is consistent with the limit on structure at 0.6 GHz.

The correlation of broadening timescales over the range from 0.3 to 1.4 GHz provides support for diffractive scattering in the nebular material. Although the simple thin-screen prediction for interstellar scattering is a single-sided exponential, $\exp(-t)$, models including two widely separated screens or a single thick screen both predict pulse shapes similar to the observed $(t/a_3)\exp(-t/a_3)$ form of the components (Williamson 1974). Isaacman & Rankin (1977) have derived parameters for a two-screen model from studies of the average pulse profile of the Crab pulsar.

A scatter plot of the 1.4 GHz component energies, $A = a_1 a_3^2$, from the fitted parameters in equation (1), versus component width, a_3, shows that the energies are independent of the pulse width, have an average of about 6.3×10^{-3} Jy-s, and are scattered over two orders of magnitude. This means that the peak flux is approximately inversely proportional to the width; stronger pulses are narrower. The data from other observing sessions show that although the broadening times change, the pulse energies remain within the same range; i.e., when the scattering times are longer, the peak amplitudes are correspondingly smaller. This multiepoch result supports the hypothesis that, in spite of questions about the pulse component shape and the frequency dependence of the exponential decay timescale, the shape of the components at 1.4 GHz is most likely the result of scattering by the intervening medium.

The wide variations in pulse broadening seen within a single pulse are, however, difficult to explain unless the scattering screen is illuminated differently by each component. While we expect variation in the pulse broadening from component to component and from pulse to pulse owing to their being instantaneous samplings of the time-variable diffractive effects, why does the *minimum* exponential timescale of the components at 1.4 GHz agree with that extrapolated from 0.3 GHz? We have considered the possibility that the components of giant pulses are intrinsically single impulsive events that are multiply refracted and/or diffracted by discrete regions of enhanced plasma density and/or turbulence, respectively. Lyne & Thorne (1975) invoked similar intermittency in the wave-front perturbing medium to explain the irregular and rapidly varying effects of the 1974 event, and Cordes, Hankins, & Moffett (1998) have studied the effects of discrete, small-scale "screenlets" on giant pulses. An intermittent scattering medium that multiply refracts and/or diffracts a single impulsive signal appears to solve the problem, but has serious difficulties in explaining the frequency independence of the spread and the multiplicity of pulse components.

Consider a screen at a distance xD from the pulsar and $(1-x)D$ from the observer. Diffraction leads to an expansion of the angular spectrum of the intensity by an angle $\theta_d \equiv \lambda/l_o$ where l_o is the coherence scale for one radian of phase difference across the wavefront. An impulse that passes through this screen is broadened by the multipath diffractive timescale, τ_d. If the scattering material covers a transverse scale of $l_d = xD\theta_d$ centered on the geometric line of sight, then $\tau_d = x(1-x)D\theta_d^2/2c$. A measure of the apparent angular size of the pulsar is $\theta_{o,d} = x\theta_d$. If τ_d is 4 μs at 1 GHz and the screen is located 2 pc from the pulsar,

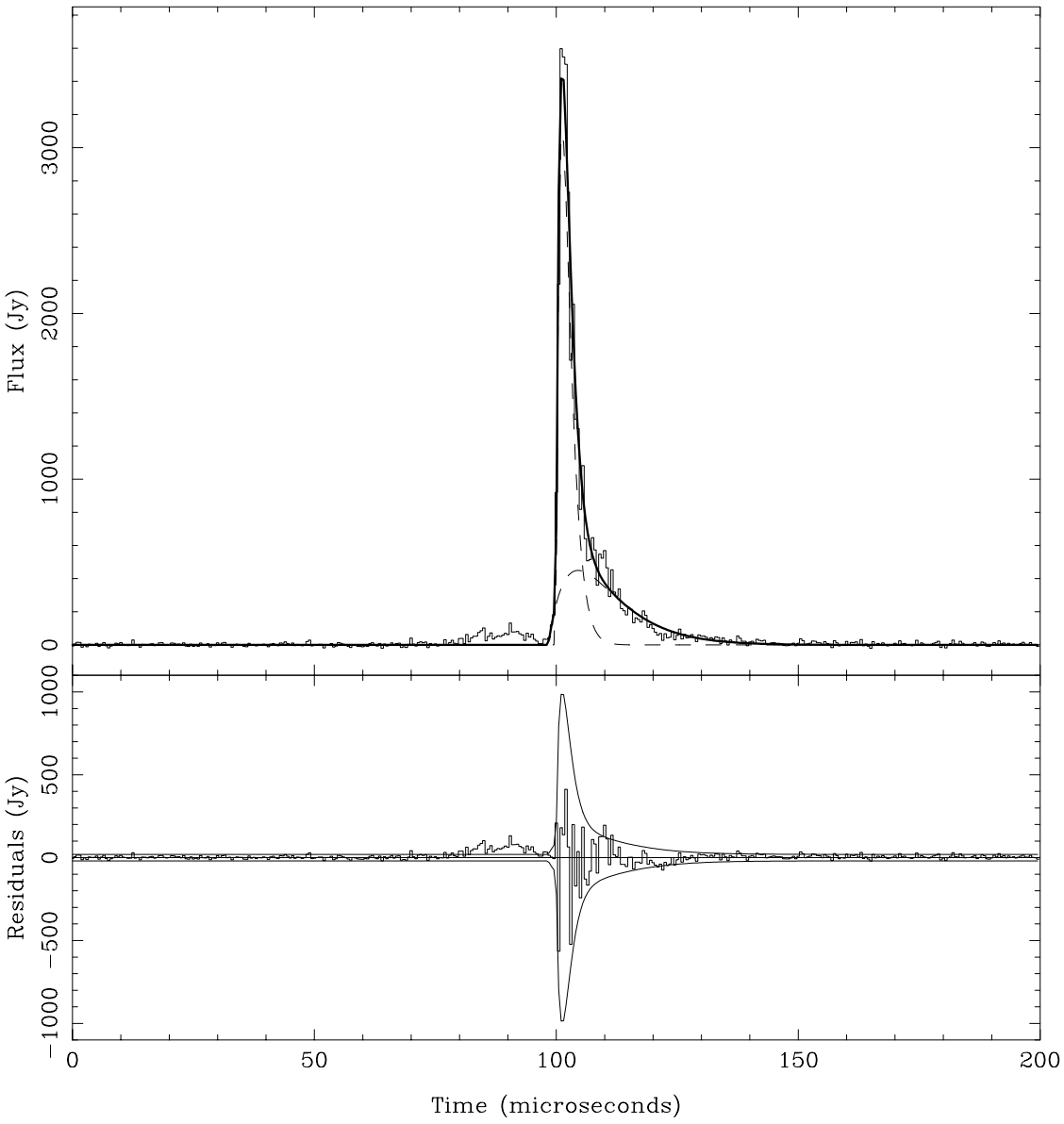

FIG. 4.—An example of a simple 1.4 GHz single-pulse profile. The intensity data are modeled by the dark solid line, which is created using the fitted components represented by the dashed lines. These components are characterized by a fast, nearly linear rise, followed by an exponential decay. The narrow component of the giant pulse shown here has a characteristic timescale of 1.2 μs. The fit residuals are shown in the lower panel with the 2 σ uncertainty envelope shown, where $\sigma = (T_{\rm sys} + T_{\rm pulsar})(\Delta\nu\,\Delta\tau)^{-1/2}$, and $\Delta\nu$ and $\Delta\tau$ are the receiver bandwidth and postdetection integration time, respectively.

$x = 10^{-3}$, $\theta_d = 60$ mas, $\theta_{o,d} = 60$ μas, $l_o = 10^7$ cm, and $l_d = 1.8 \times 10^{11}$ cm. If the diffracting material covers only a fraction of l_d, then the pulse broadening time will be *reduced* relative to τ_d because of the reduction in the multipath propagation (Cordes et al. 1998). The observed frequency scaling between the 0.3 and 1.4 GHz broadening times reported above is not consistent with this result. In addition, a diffracting region not located along the line of sight will result in components disappearing from view as the frequency increases, owing to the reduced viewing zone set by l_d centered on the line of sight. This is in conflict with the current observational results.

Refraction in an intermittent medium has limitations similar to those of diffraction. Consider a uniform-density, spherical plasma lens at a transverse distance b from the line of sight, with a transverse dimension significantly less than b. The excess propagation delay from the pulsar to the observer is dominated by the geometric delay, $\tau_g = b^2/[2cx(1-x)D]$, and is independent of frequency, owing to the highly aberrant lens. While multiple lenses of this form appear to satisfy the frequency independence of giant pulse component spacings, they will *not* satisfy the frequency independence of the number of components and their overall distribution in longitude. More components over a wider range of longitude would be expected at lower frequencies, as is the case for diffraction discussed above.

We conclude that the multiplicity of components is intrinsic to the pulsar emission mechanism or to propagation effects within the pulsar magnetosphere. Multiple scatterings of a single emitted pulse component cannot easily explain the observed spread and multiplicity of pulse components. Despite this, we favor propagation effects in the Crab Nebula as an explanation for the shape of the components at 1.4 GHz and below. Alternatively, the observed

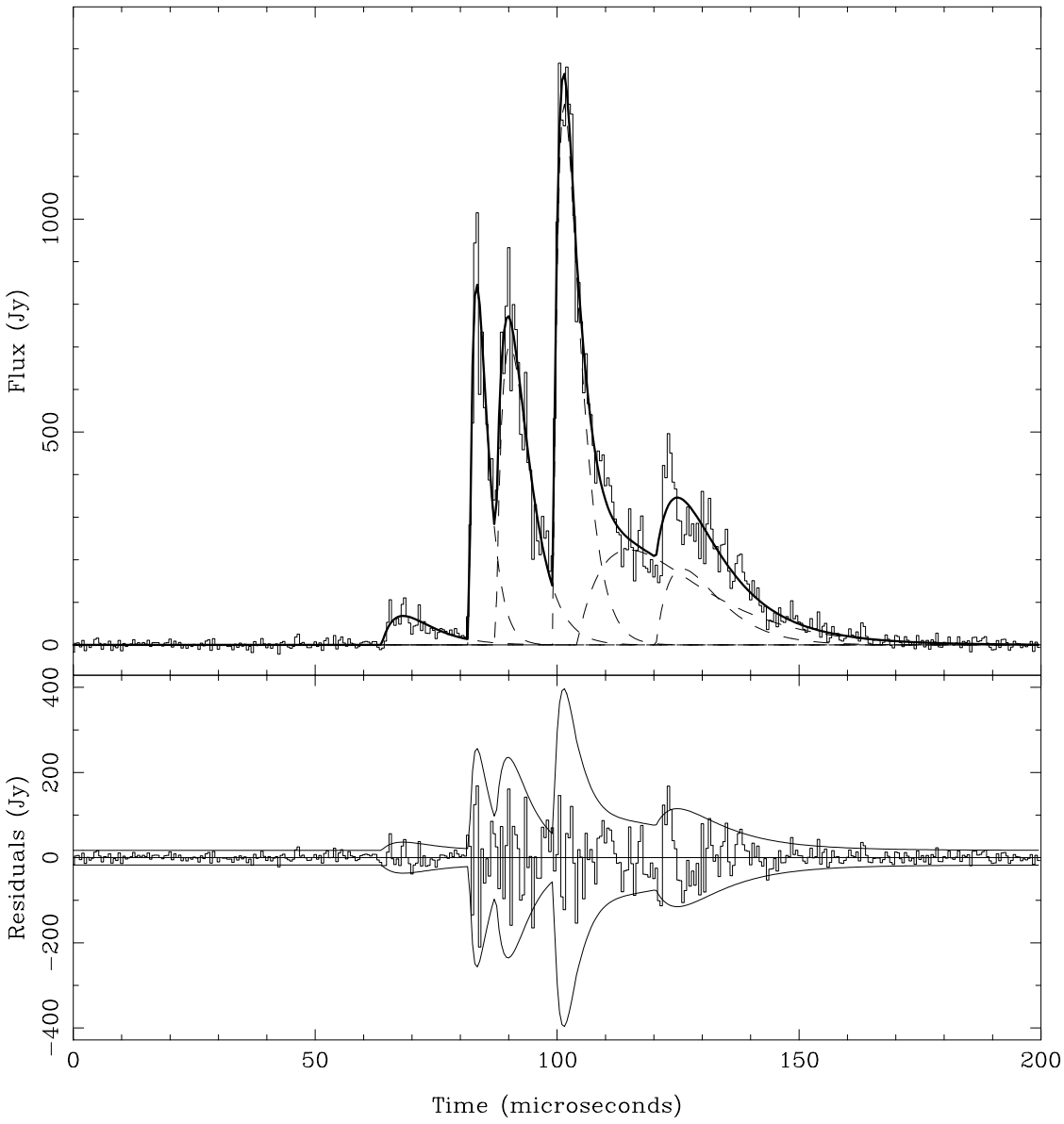

FIG. 5.—An example of a complex 1.4 GHz single-pulse profile. The intensity data are modeled as described in Fig. 4. The final component of the giant pulse shown here has a characteristic timescale of 5.7 μs. The fit residuals are as described in Fig. 4.

component shape may be intrinsic to the emission. Each component is emitted with its own timescale, but the characteristic (t/a_3) exp $(-t/a_3)$ shape. Components with timescales shorter than the interstellar broadening timescale are broadened by scattering in the ISM. This model explains the observed correlation between the minimum timescale and the low-frequency scattering, but involves two separate explanations for the characteristic shape of the components. Determining whether the long-τ end of the distribution scales with the low-frequency scattering or is independent of it would distinguish between the two possibilities. Observations at multiple frequencies during times of minimal scattering at 0.3 GHz are critical to further inquiry.

3.4. *Energies and Spectral Indices*

The distribution of pulse energy amplitudes from the 1.4/0.6 GHz experiment are displayed along with the corresponding detection thresholds in Figure 7. The 1.4 GHz amplitudes of the 13 pulses that were not detected at 0.6 GHz are also shown. Solid lines corresponding to spectral indices of -2.2 and -4.9 are shown, where spectral index q is defined by $A_{\rm GB}/A_{\rm VLA} = (0.6/1.4)^q$. The overall spectral index for the Crab pulsar is -3.1, while the spectral index for the average main pulse, which is shown as a dotted line in Figure 7 (Moffett 1997), is -3.0. The pulse amplitude of the average main pulse is 5.4×10^{-3} Jy-s at 0.6 GHz. The largest 0.6 GHz giant pulse therefore has a pulse amplitude of about 150 times the amplitude of the average pulse. The giant pulses are narrower than the average pulse, and so are even stronger relative to the average pulse within this window.

Lundgren et al. (1995) concluded from their analysis of the relative contribution of giant pulses to the average as a function of frequency (cf. § 1) that if the emission is narrowband, the rate of giant pulses must increase with frequency, while if the emission is broadband, then the giant pulses must have flatter spectra than the weak pulses. Heiles & Rankin (1971) found that their measured spectral indices at

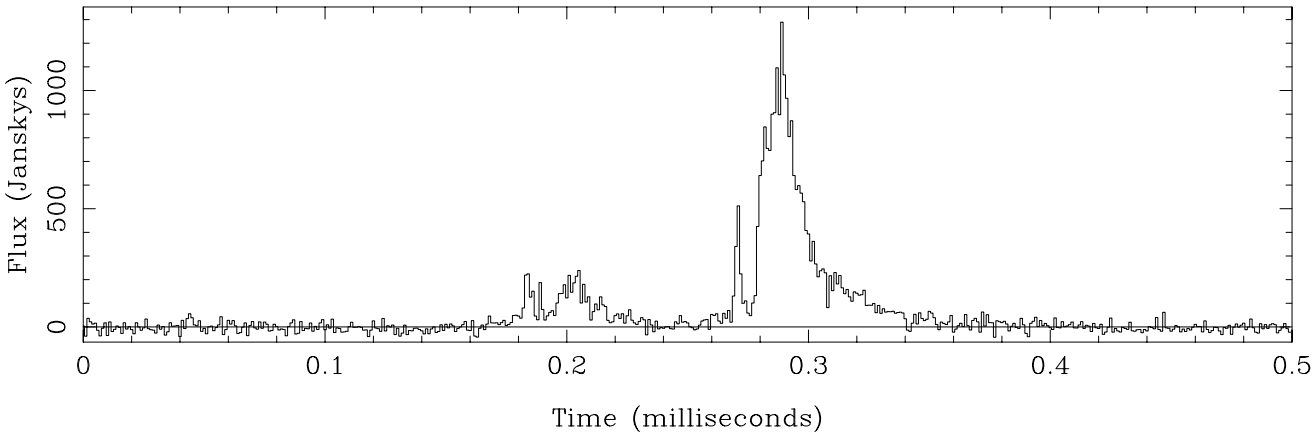

FIG. 6*a*

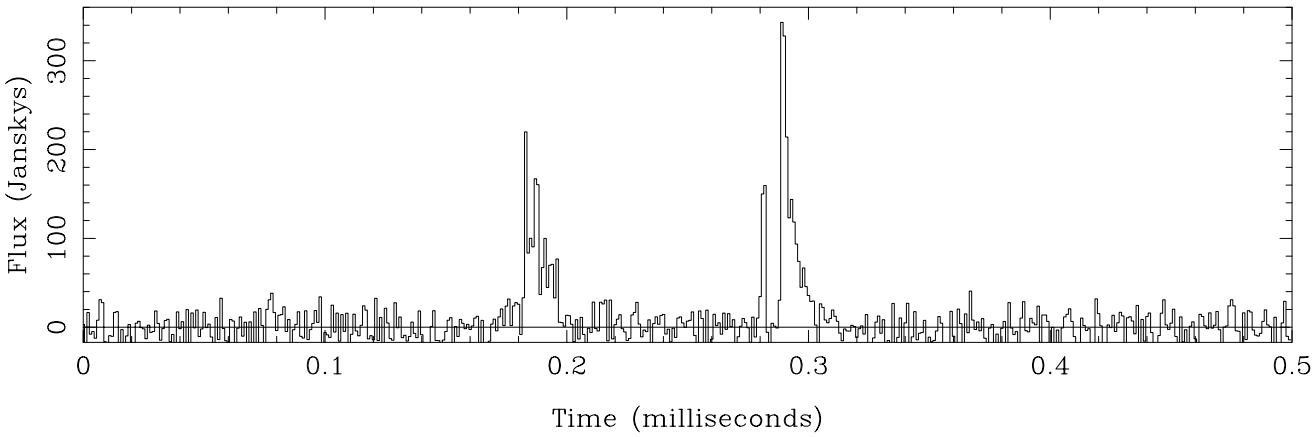

FIG. 6*b*

FIG. 6.—(*a*) Single giant pulse recorded at 4.8851 GHz, plotted with 1 μs resolution. (*b*) The same pulse recorded at 1.4351 GHz, plotted with the same time resolution.

low radio frequencies ranged from nearly 0 to less than -3.0. Similarly, Moffett (1997) found that between 1.4 and 4.9 GHz, giant pulse spectral indices ranged from 0 to -4, with an average of about -2. These two studies corroborate Lundgren's analysis. We find that at least 70% of the pulses are broadband, and so we expect that their spectral indices are, on average, flatter than the average main pulse spectral index.

The average spectral index of the giant pulses in Figure 7 that were detected at both frequencies is -3.4, which is comparable to that of the average main pulse. This estimate is biased by the fact that the pulses that were not detected at 0.6 GHz have flatter spectral indices. In addition, there may be systematic errors in flux calibration that could change the average spectral index by up to 0.4.

The individual giant pulse spectral indices display a relatively large scatter. Individual pulse spectral indices are known for two other pulsars. The distributions of spectral indices for pulsars B0329+54 and B1133+16 have a standard deviation of 0.2, and range from -1.6 to -3.1 and -2 to 0, respectively (Bartel & Sieber 1978). One contribution to the spectral index variations is the stochastic uncertainty in the determination of the amplitudes that is introduced by the low number of degrees of freedom in narrowband observations of intrinsically short duration pulses. We estimate this uncertainty to be of the order of 10% at 1.4 GHz and 20% at 0.6 GHz for an intrinsic pulse width of 1 μs. This is not large enough to explain the scatter in the spectral indices. The scatter could also be intrinsic to the radiation emission process. The signal could consist of a randomly occurring series of nanosecond impulses whose combined power spectrum is irregular. This would cause scatter in the observed spectral indices. But with the radiation extending over 1 μs or more, there are many nanosecond pulses which would smooth out this distribution. Alternatively, one might expect the spectral index to vary because of properties of the emission beam, such as frequency dependence and orientation with respect to the observer. Future observations with higher time resolution and also with many samples across the spectrum will provide critical new insight into the giant pulse emission process.

3.5. *Models of the Emission Beam*

We consider two general models for giant pulse emission. In the temporal model, the giant pulse emission components are impulses in time (<1 μs), with angular beam widths comparable to that of the average pulse, $\sim 3°$. Following Lundgren (1994), we also consider a model in which the enhanced emission during a giant pulse results from a steady narrow beam ($<1'$) whose position wanders on timescales of 300 μs $\ll t \ll P$. In this case, intrinsic structure within a particular giant pulse is due to structure within this

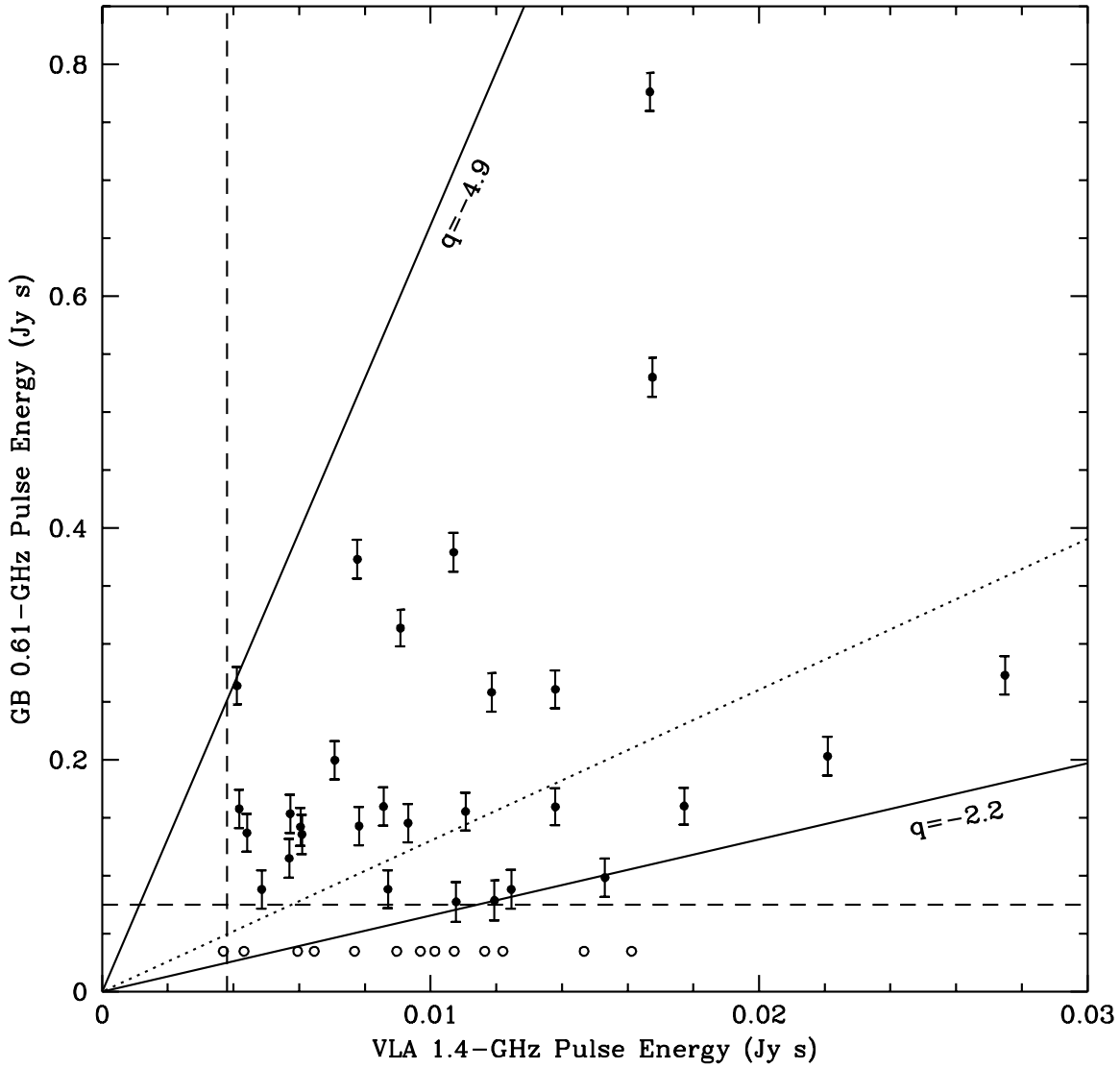

FIG. 7.—Pulse energy amplitudes in Jy-s at 0.6 and 1.4 GHz. The filled circles denote the 29 pulses that were detected at both frequencies. Error bars reflect the measurement uncertainty, which is negligible for the 1.4 GHz data. Uncertainty in the telescope gain calibration used at 0.6 GHz introduces an additional systematic uncertainty of 50%. The open circles represent those pulses seen at 1.4 GHz that were certainly not detected at 0.6 GHz. The horizontal dashed line represents the cutoff of 0.075 Jy-s, below which we could not detect pulses at 0.6 GHz. The vertical dashed line indicates our estimate of the VLA threshold, corresponding to 6 times the rms noise. The one pulse with a 1.4 GHz energy less than this occurred while our threshold was set to 5 times the rms noise. The solid lines represent spectral indices of $q = -2.2$ and $q = -4.9$. The dotted line indicates the average main pulse spectral index.

narrow beam. In both models, the average beam may be circular, as in polar cap models, or fan-shaped, as is likely if the emission comes from the outer gaps.

In the angular model, the narrow beam of emission may wobble in either the l direction (along the trajectory of the line of sight), or the ϕ direction (perpendicular to the trajectory of the line of sight). The width of the giant pulses corresponds to the size of the beam in this model, while the jitter in arrival times, $\sigma_{\rm toa}$, corresponds to the wobbling of the beam along l. For giant pulses that occur a fraction f of the time, the wobble in ϕ is then $w_{\rm GP}/(Pf)$, where P is the pulse period (following Lundgren et al. 1995). Lundgren was able to separate the giant pulse and normal pulse distributions at 0.8 GHz, and found that one of 40 pulses is giant. Since the giant pulses form a separate distribution, then if they are all broadband, they will all also appear at higher radio frequencies. Then at 1.4 or 4.9 GHz, 1 of 40 pulses should be giant. In fact, Moffett (1997) finds that 1 of 50 pulses at 1.4 GHz has an energy greater than 20 times the average. At 4.9 GHz, the intrinsic width of the giant pulses is 0.1–0.4 μs. We find $\sigma_{\rm toa} \approx 100$ μs, so the 0°.001 to 0°.004 beam must wobble 1°.1 in l and 0°.05 to 0°.2 in ϕ. This is not consistent with a narrow beam wobbling within a roughly circular average beam.

3.6. *The Emission Mechanism*

Radio emission from pulsars must come from a coherent emission process (Cordes 1981). The exact process is very uncertain, as is the location(s) of the emission. It is not necessary for the giant pulse emission to originate at the same place or in the same way as the ordinary pulse emission. The broadband nature of the giant pulse emission provides the main constraint on its origin. According to Melrose (1996), broadband emission is traditionally associ-

ated with models in which the emission occurs at a pair-production front in the polar cap, or by Schott radiation from a corotating charge and current distribution outside the light cylinder (e.g., da Costa & Kahn 1985; Ardavan 1992, 1994). The emission process itself could rely on plasma instabilities (Cheng & Ruderman 1977; Asséo 1993; Machabeli & Usov 1979; Kazbegi et al. 1991; Weatherall 1996). Alternatively, other maser processes, such as linear acceleration emission (Melrose 1978; Rowe 1995) or maser curvature emission (Luo & Melrose 1992, 1995), could produce the radiation. In any case, if the giant pulses are a temporal effect, this variability in radio emission could be the result of the statistics of a small number of coherently emitting regions that are incoherently summed, or an increase in the coherence within a single emission region.

Although we believe that the $(t/a_3)\exp(-t/a_3)$ characteristic shape of the giant pulse components at 1.4 GHz is most likely the effect of propagation through the Crab nebula interface, the remaining questions (see § 3.3) lead to consideration of effects intrinsic to the pulsar. An asymmetric shape is not expected for a simple narrow beam with an angular wobble. In either the temporal or angular beam model, this shape might be explained by effects that occur as the signals traverse the pulsar magnetosphere (Eilek 1999). The effects of aberration are too small to produce the broadening and asymmetry seen in these pulses, if one confines the range of emission altitudes to 4.5 km, the limit obtained from the timing residual differences at the two frequencies. In the temporal model, the asymmetric shape is consistent with any emission process that turns on with a rapid nearly linear rise, then saturates and decays. In this case, one might expect the peak energy to be independent of width, whereas we have seen that it is the total pulse energy which is independent of width.

If the model is truly temporal, then the angular size of the beam does not affect the observed pulse width. The radiation is beamed into a beam width $\theta \approx \gamma^{-1}$. The beam must be wider than any given 1.4 GHz pulse component, 50 μs, and therefore $\gamma \lesssim 100$. We can use this value of γ to estimate particle properties using a simplistic model of coherent curvature radiation. The power lost by the N excess charged particles in the bunch will be

$$P_{\rm curv} = N^2\left(\frac{2e^2\gamma^4 c}{3\rho_c^2}\right),$$

where e is the charge on an electron, γ is the relativistic factor $(1 - v^2/c^2)^{-1/2}$, and ρ_c is the radius of curvature of the magnetic field. We observe 6.3×10^{-3} Jy-s in a 50 MHz band, so $P_{\rm curv}$ must equal the measured luminosity, which is therefore greater than 3.9×10^{23} ergs s^{-1}, assuming a distance of 2 kpc and a circular beam 300 μs = 3° wide. Then the number of particles in the bunch must be at least

$$N = 9.2 \times 10^{19}\left(\frac{\gamma}{100}\right)^{-2}\left(\frac{\rho_c}{10^8\ {\rm cm}}\right).$$

These particles must fit within a cube with volume $\leq \lambda_{\rm obs}^3$ in order to maintain the observed coherence, so the number density of excess charges must be at least $\delta n_e = N/\lambda_{\rm obs}^3 = 9.9 \times 10^{15}(\gamma/100)^{-2}$ cm^{-3} for the parameters used above and a wavelength of 21 cm. For comparison, the Goldreich-Julian density in the observer's frame is $n_{\rm G\text{-}J} = \Omega B/e2\pi c = 8.3 \times 10^{12}(R/R_{\rm NS})^{-3}$ cm^{-3}, using a surface magnetic field of 4×10^{12} G. The excess charge density can be further reduced if several bunches are radiating in a periodic structure.

4. SUMMARY

The giant pulse emission from the Crab pulsar is broadband, since 70% of the pulses are observed in our 1.4/0.6 GHz experiment. The strong correlation in arrival times at the two frequencies implies that the same radiating unit is operating at both frequencies. The giant pulses display a scatter in spectral index that is consistent with or flatter than the spectral index of the average main pulse component. Pulsar emission models are restricted to those that can explain the broadband nature of the giant pulse radiation on intrinsic observed timescales of 1 to 10 μs.

Above 1 GHz, a multiplicity of components is observed with frequency-independent spacing and number. The 1.4/0.6 GHz data are also consistent with frequency independence. We conclude that the multiplicity is intrinsic to the pulsar emission process and not the result of multiple imaging in the intervening plasma.

The exponential pulse-broadening timescale of the average pulse at 0.3 GHz and of the giant pulses at 0.6 GHz are consistent with multipath propagation effects. The large values and rapid variations indicate a special scattering region. We identify this region with the interface between the Crab synchrotron nebula and the surrounding supernova ejecta. At 1.4 GHz, the observed giant pulse component shapes are characterized by fast rise and exponential decay timescales that are correlated. The minimum timescale is consistent with extrapolation of the pulse broadening at lower frequencies with a filled turbulent-scattering screen. The shape and distribution of the broadening at 1.4 GHz are not fully understood. Multifrequency simultaneous observations of giant pulses with higher time resolution at epochs of minimal scattering at low frequency will provide critical new insights into the emission processes and subsequent propagation effects.

We thank John Ford for assistance with the trigger reception software. Thanks to the observatory staff at both sites for minimizing Internet traffic during the two hours of the experiment. T. H. Hankins and D. A. Moffett thank the NSF for partial funding of this work under grant AST 93-15285. D. C. Backer and S. Sallmen thank the NSF for partial funding of this work under grant AST 93-07913. We are indebted to NASA for maintenance of the 25 m telescope at Green Bank. We thank J. Cordes, R. Jenet, M. Kramer, A. Melatos, and J. Weatherall for conversations and comments on the early versions of the paper, and the referee for attentive reading and useful criticism.

REFERENCES

Ardavan, H. 1992, in IAU Colloq. 128, Magnetospheric Structure and Emission Mechanisms of Radio Pulsars, ed. T. H. Hankins, J. M. Rankin, & J. A. Gil (Poland: Pedagogical Univ. Press), 316
———. 1994, MNRAS, 268, 361
Argyle, E., & Gower, J. F. R. 1972, ApJ, 175, L89
Asséo, E. 1993, MNRAS, 264, 940
Backer, D. C., Dexter, M., Zepka, A., Ng, D., Wertheimer, D. J., Ray, P. S., & Foster, R. S. 1997, PASP, 109, 61
Backer, D. C., & Wong, T. 1996, in IAU Colloq. 160, Pulsars: Problems and Progress, ed. S. Johnston, M. A. Walker, & M. Bailes (San Francisco: ASP), 87
Bartel, N., & Sieber, W. 1978, A&A, 70, 307

Cheng, A., & Ruderman, M. A. 1977, ApJ, 212, 800
Comella, J. M., Craft, H. D., Lovelace, R. V. E., Sutton, J. M., & Tyler, G. L. 1969, Nature, 221, 453
Cordes, J. M. 1981, in IAU Symp. 95, Pulsars: 13 Years of Research on Neutron Stars, ed. W. Seiber & R. Wielebinski (Dordrecht: Reidel), 115
Cordes, J. M., Hankins, T. H., & Moffett, D. 1998, in preparation
da Costa, A. A., & Kahn, F. D. 1985, MNRAS, 215, 701
Eilek, J. A. 1996, in IAU Colloq. 160, Pulsars: Problems and Progress, ed. S. Johnston, M. A. Walker, & M. Bailes (San Francisco: ASP), 155
———. 1999, ApJ, submitted
Friedman, J., & Boriakoff, V. 1990, in Proc. IAU Colloq. 128, Magnetospheric Structure and Emission Mechanisms of Radio Pulsars, ed. T. H. Hankins, J. M. Rankin, & J. A. Gil (Poland: Pedagogical Univ. Press), 347
Goldstein, S. J., & Meisel, D. D. 1969, Nature, 224, 349
Hankins, T. H. 1971, ApJ, 169, 487
Hankins, T. H., & Moffett, D. A. 1998, BAAS, 30, 903
Hankins, T. H., & Rickett, B. J. 1975, Methods Comput. Phys., 14, 55
Heiles, C., Campbell, D. B., & Rankin, J. M. 1970, Nature, 226, 529
Heiles, C., & Rankin, J. M. 1971, Nature, 231, 97
Hester, J. J., et al. 1996, ApJ, 456, 225
Isaacman, R., & Rankin, J. M. 1977, ApJ, 214, 214
Kazbegi, A., Machabeli, G., Melikidze, G., & Shukre, C. 1991, A&A, 309, 515
Lundgren, S. C. 1994, Ph.D. thesis, Cornell Univ.
Lundgren, S., Cordes, J. C., Ulmer, M., Foster, R., & Hankins, T. H. 1995, ApJ, 453, 433
Luo, Q., & Melrose, D. B. 1992, MNRAS, 258, 616
———. 1995, MNRAS, 276, 372
Lyne, A. G., & Thorne, D. J. 1975, MNRAS, 172, 97L
Machabeli, G. Z., & Usov, V. V. 1979, Soviet Astron. Lett., 5, 238
Melrose, D. B. 1978, ApJ, 225, 557
———. 1996, in IAU Colloq. 160, Pulsars: Problems and Progress, ed. S. Johnston, M. A. Walker, & M. Bailes (San Francisco: ASP), 139
Moffett, D. A. 1997, Ph.D. thesis, New Mexico Inst. Mining and Technology
Moffett, D. A., & Hankins, T. H. 1996, ApJ, 468, 779
Romani, R., & Yadigaroglu, I.-A. 1995, ApJ, 438, 314
Rowe, E. T. 1995, A&A, 296, 275
Staelin, D. H., & Reifenstein, E. C. 1968, Science, 162, 1481
Staelin, D. H., & Sutton, J. M. 1970, Nature, 226, 69
Sutton, J. M., Staelin, D. H., & Price, R. M. 1971, in IAU Symp. 46, The Crab Nebula, ed. R. D. Davies & F. G. Smith (Dordrecht: Reidel), 97
Taylor, J. H., & Weisberg, J. M. 1989, ApJ, 345, 434
Weatherall, J. C. 1996, in IAU Colloq. 160, Pulsars: Problems and Progress, ed. S. Johnston, M. A. Walker, & M. Bailes (San Francisco: ASP), 205
Williamson, I. P. 1974, MNRAS, 166, 499